JOURNAL OF MOLECULAR SPECTROSCOPY 150, 201–217 (1991)

Preliminary Analysis of the Pentad of $^{13}CH_4$ from Raman and Infrared Spectra

J. M. JOUVARD,[1] B. LAVOREL,[1] AND J. P. CHAMPION[1]

Laboratoire de Spectronomie Moléculaire et Instrumentation Laser, Université de Bourgogne, U.A CNRS N° 777, 6 Boulevard Gabriel, 21100 Dijon, France

AND

L. R. BROWN

Jet Propulsion Laboratory, California Institute of Technology, 4800 Oak Grove Drive, Pasadena, California 91109

Preliminary results on the simultaneous analysis of infrared and Raman data of $^{13}CH_4$ in the 3-μm region (ν_1, ν_3, $2\nu_2$, $\nu_2 + \nu_4$, and $2\nu_4$) are presented. The infrared spectrum of $^{13}CH_4$ (90% enriched) has been recorded with the Fourier transform spectrometer at Kitt Peak National Observatory. Line positions have been measured with a relative accuracy of 0.0001 cm^{-1} (for well-isolated lines) using 0.0118-cm^{-1} resolution spectra. In order to compensate for the lack of infrared information about low J transitions of vibrational bands forbidden in infrared, two spectra of the ν_1 (A_1) and $2\nu_2$ (A_1) Q branches have been recorded in Dijon by inverse Raman spectroscopy with an instrumental resolution of 0.0022 cm^{-1}. Line positions have been measured with a precision of 0.001 cm^{-1} using a profile fitting procedure. Raman and infrared data were combined in a weighted least-squares fit to determine vibration–rotation constants. We used an effective tensorial Hamiltonian taking into account all interactions within the pentad up to the fourth order of approximation. The preliminary analysis has been carried out throughout $J = 13$ involving 1200 data reproduced with a standard deviation of 0.0007 cm^{-1}, approximately 30 times better than the most recent results published on the $^{12}CH_4$ pentad. © 1991 Academic Press, Inc.

INTRODUCTION

It is very difficult to model to within experimental uncertainties the high accuracy positions and linestrengths of methane that are routinely obtained from Fourier transform spectrometers (FTS). It is thought that successful analyses can ultimately be achieved through simultaneous treatment of band systems (so-called polyads). Recently the three lowest levels (the vibrational ground state and the ν_2 and ν_4 fundamentals) of $^{12}CH_4$ and $^{13}CH_4$ were analyzed (*1, 2*) to reproduce high accuracy data (6×10^{-5} cm^{-1} for positions and 3–4% for linestrengths). The next higher polyad, the pentad, contains five interacting states (ν_1, ν_3, $2\nu_2$, $\nu_2 + \nu_4$, and $2\nu_4$) that give rise to transitions between 5 and 3 μm. Prior analyses of $^{12}CH_4$ made several years ago with high accuracy line centers (*3–7*) failed to reproduce the experimental data by two orders of magnitude, although much of the methane spectrum was assigned (*4, 8, 9*), and a good under-

[1] Electronic mail address: SMIL@FRCCUB11.

0022-2852/91 $3.00

standing of the vibration–rotation interactions was achieved (*3, 4*). Much less attention was given to the $^{13}CH_4$ pentad. Experimental positions, assignments, and some linestrengths were reported for ν_3 (*10, 11*), ν_1 (*12*), and $2\nu_4$ and $\nu_2 + \nu_4$ (*8, 9*) covering transitions of intermediate values of J. Any published attempts to model these measurements were solely based on isolated band studies.

Encouraged by the recent success with the dyad bands of methane and the pentad bands of two heavier spherical tops (*13, 14*), we are engaged in a new analysis of the pentad region of methane. A revised theoretical approach based on the model used by Poussigue *et al.* (*3*) is being used, but in this effort, the Hamiltonian is expanded to fourth order, and the recent understanding about the proper reduction of the effective Hamiltonian is applied. The long term goal is to model positions and linestrengths of both isotopes, as was done for the dyad. Since no thorough assignment of the $^{13}CH_4$ pentad has been made, this preliminary study is being done first so that weak lines in the natural sample spectrum can be identified. For this, infrared spectra have been recorded at 0.011-cm^{-1} resolution using the FTS at Kitt Peak National Observatory/National Solar Observatory. However, two of the bands, ν_1 and $2\nu_2$, are forbidden in the infrared, and their weak absorptions appear at higher J only through the interactions. To access their low J transitions, stimulated Raman spectra in their Q-branch regions have been recorded at Dijon at 0.002-cm^{-1} resolution. From the complementary datasets, reliable values of all lower-order Hamiltonian parameters were determined so that the infrared spectrum could be efficiently assigned from the resulting prediction. In the present study, we report the Raman observations and discuss the success and limitations of the revised theoretical approach.

EXPERIMENTAL DETAILS

Two infrared and Raman spectra have been used in the analysis of the $^{13}CH_4$ pentad; their gas conditions are shown in Table I. The instrumentation has been described elsewhere for both the FTS at KPNO/NSO (*15*) and the inverse Raman spectrometers at Dijon (*14*) so that only specific details relevant for the present study need to be described here.

TABLE I

Experimental Conditions of the Raman and Infrared Data

Type	Path (m)	Pressure (Torr)	Temp (K)	$^{13}CH_4$ Purity	Band Pass (cm^{-1})
Infrared	0.25	5.93	296	99%	1800-5100
Infrared	2.39	7.88	296	99%	1800-5100
Raman	(a)	3.3	293	90%	(b)
Raman	(a)	36.	293	90%	(b)

(a) The path length for Raman experiment is not known since the scattered light comes from a narrow area on which the laser is focused.
(b) See Ref. (*14*) for details.

Infrared Data

These data are part of a large set of $^{12}CH_4$, $^{13}CH_4$, and CH_3D spectra recorded at 0.011-cm^{-1} resolution (unapodized) using a CaF_2 beamsplitter in the FTS at KPNO/NSO. An integration time of ≈ 1 hr was used with InSb detectors to achieve a signal-to-noise ratio of 300:1 or better for a band pass of 1800 to 5100 cm^{-1}. To reach the FTS, a beam from a globar source passed through two absorption cells of different lengths: 0.05 and 2.39 m or 0.25 and 1.5 m. Generally, one cell contained the methane sample and the other the calibration sample (CO or CO_2). The gas pressures were monitored with Baratron capacitance gauges, and sample temperatures were inferred from the temperature of the cell exterior. An isotopically enriched sample of "99%" $^{13}CH_4$ from Cambridge Isotope Laboratories was used. Two impurities in this sample have been identified by spectroscopic analysis: 0.5% $^{12}CH_4$ and 0.2% $^{13}CO_2$. Figure 1 shows the Q-branch region of the ν_3 bands of both isotopes as observed in the first spectrum in Table I.

The line centers were found by doing first and second derivatives of the apodized spectrum. For the first infrared scan shown in Table I, the 1.5-m cell contained 1.6 Torr of CO at 296 K to provide the calibration of positions using the 2–0 band (*16*) at 4260 cm^{-1}; the rms of 24 CO lines was 0.00005 cm^{-1}. The calibration was then checked using the ν_3 Q- and R-branch lines of $^{12}CH_4$. The other scan was calibrated using isolated ν_3 lines of both isotopes. Based on combination differences, the precision is 0.0001 cm^{-1} or better for isolated transitions and perhaps ± 0.0040 cm^{-1} for badly

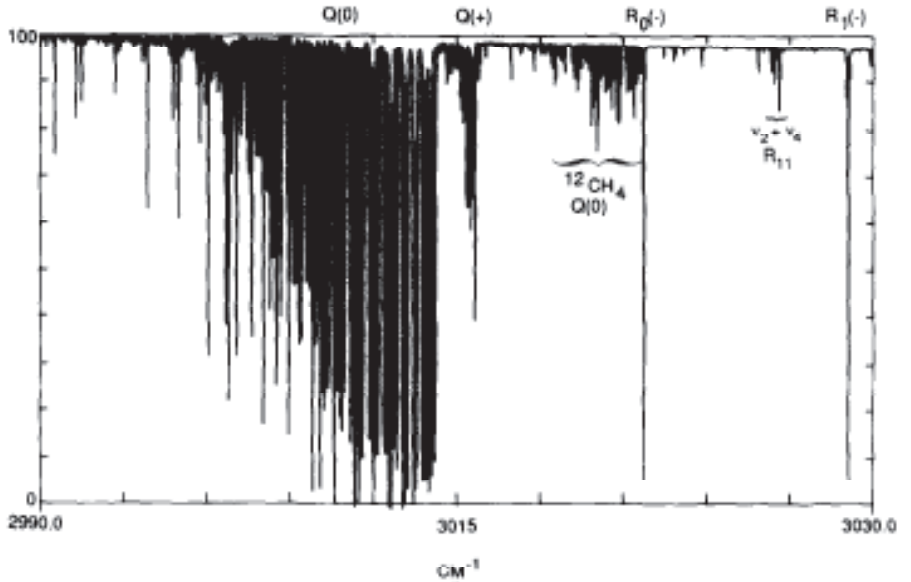

FIG. 1. The observed infrared spectrum of isotopically enriched methane in the ν_3 region. The gas pressure is 5.93 Torr and the path is 0.25 m. The apodized spectrum has an effective resolution of 0.016 cm^{-1}. The interval contains the allowed $Q(0)$ and forbidden $Q(+)$ branches of $^{13}CH_4$ (at 3010 and 3012 cm^{-1}, respectively), the allowed $Q(0)$ branch of ν_3 of $^{12}CH_4$ at 3019 cm^{-1}, allowed $R(-)$ lines of ν_3, and some higher J lines (R_{11}) of $\nu_2 + \nu_4$.

blended features. However, based on recent work with foreign-broadened methane in the ν_3 region (*17*), it is reasonable to expect that the pressure (self-) shifts are on the order of 10^{-5} cm^{-1}/Torr and depend on the rotational quantum numbers of the transitions. Unfortunately, no shift correction can be attempted at this time, so that the absolute accuracies of ± 0.00015 cm^{-1} are assumed for the line positions.

Raman Data

In the inverse Raman configuration employed in the present study, a probe laser (single mode cw argon laser) and a pump laser (a pulse amplified dye laser) were focused and mixed in a 90% enriched methane sample. The power of the cw and pulsed sources were respectively 0.4 W and 350 kW. The argon laser was tuned to the blue line at 488 nm. The Raman signal was detected on the probe laser by a fast photodiode and a boxcar averager.

The overtone band $2\nu_2$ of isotopic species of methane is a weak feature in the Raman spectrum. The $2\nu_2(A_1)$ component has been recorded in $^{13}CD_4$ (*14*) with experimental conditions at the limit of the sensitivity of the experiment: average over a great number of shots (32) and a 150-Torr pressure limiting the resolution. The advantages of a multiple pass cell in stimulated Raman spectroscopy have been recently demonstrated in Dijon (*18*). The enhancement of the signal-to-noise ratio can reach a factor of 22 for 44 passes. Consequently, our multiple pass cell was filled with the gas sample at room temperature and at pressures of 34–36 Torr for the recording of the $2\nu_2$ band and 3.3 Torr for the ν_1 band (without multiple passes in the latter case) (Figs. 2–4). The Raman signal was averaged over only four laser shots for $2\nu_2$ and eight laser shots for ν_1. As shown by the upper traces on Figs. 2 and 3, the use of such a cell greatly increases the sensitivity of the Raman experiment. However, during the recording of $2\nu_2$, the coating of the cell mirrors was damaged by the scattering of the laser beams. Consequently, the Raman signal intensity measured by the photodiode was weakly perturbed, as evidenced by the nonflat baseline of the Raman spectrum of $^{13}CH_4$ in this region (Fig. 2). This feature could not allow accurate determination of Raman intensities of $2\nu_2$.

The absolute frequency calibration of the Raman spectra was achieved by measuring the frequency of the tunable dye laser at each end of the scan (*19*) using a traveling Michelson wavemeter. The 488-nm argon laser was also measured. The Raman shift at each point of the scan was interpolated from transmission fringes of an étalon with a free spectral range of 300 MHz. The best accuracy attained with this procedure was about 0.0003 cm^{-1} (*19*) in reproducing *CO* standards (*20*). This value can be considered as the limit of our measurements. The estimated accuracy generally lies in the range 0.0003–0.0010 cm^{-1}, depending on signal-to-noise ratio and on Raman lineshape.

The transition frequencies have been obtained by profile fitting using a nonlinear least-squares procedure (*21*). The program was set to refine simultaneously within a given window, one constant baseline parameter, one uniform gain parameter, and three parameters for each line component: position, intensity, and width. A Voigt profile was used with a Gaussian width fixed to 5×10^{-3} cm^{-1} accounting for both apparatus function and Doppler effect. The Lorentzian width was adjusted to fit pres-

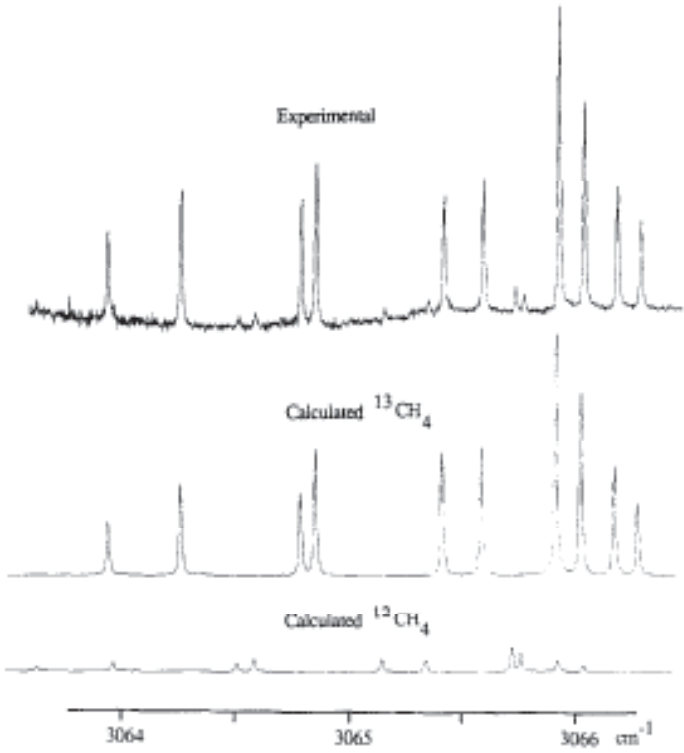

FIG. 2. Stimulated Raman spectrum of $^{13}CH_4$ (90% enriched). Scan a. (Top) Experimental spectrum using multipass cell with $T = 293$ K, $P = 34$ Torr. (Bottom) Calculated spectrum with J values up to 15.

sure broadening effects (ranging from 0.3×10^{-3} cm^{-1} for ν_1 to 3×10^{-3} cm^{-1} for $2\nu_2$ FWHM).

For well-isolated transitions, all retrievable parameters could be freely adjusted. More frequently, for blended features, appropriate constraints were applied to intensity and width parameters in order to refine transition frequencies. Figure 5 shows a typical example of profile fitting with overlapping features involving not only $^{13}CH_4$ but also $^{12}CH_4$ residuals (the line parameters of the latter were kept fixed). The constraints applied to the intensity parameters were based on predictions using one parameter each for the isotropic and anisotropic polarizabilities. Standard deviations and correlations between the retrieved parameters were used to estimate the precision of the measurements. Table II shows the experimental line centers and precision obtained for well-isolated $^{13}CH_4$ Raman lines of $\nu_1(A_1)$, $2\nu_2(A_1)$, $2\nu_2(E)$ isotropic transitions and a few $\nu_3(F_2)$ anisotropic transitions. The relative intensities listed in arbitrary units are obtained using the isotropic coefficient $\alpha_{0,1}^{A_1} = 1$ as defined in Ref. (*22*). They range from 0.3×10^{-4}–0.1×10^{-2} ($2\nu_2$) to 0.2×10^{-1}–1 (ν_1) in arbitrary units. (The other entries in Table II are discussed later). Several $Q(3)$–$Q(5)$ transitions were included in order to determine the ν_1 band origin. However, because they are often blended with other lines, these transitions have considerably poorer precision.

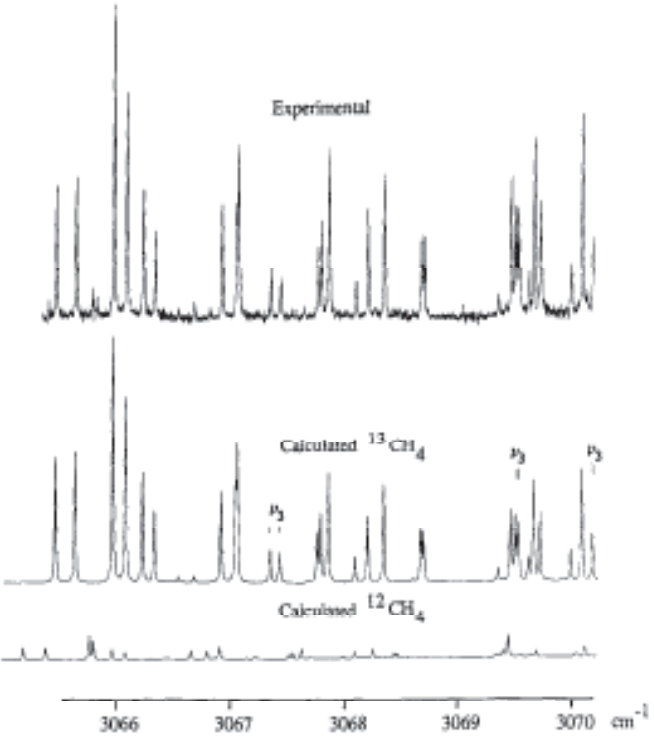

FIG. 3. Stimulated Raman spectrum of $^{13}CH_4$ (90% enriched). Scan b. (Top) Experimental spectrum using multipass cell with $T = 293$ K, $P = 36$ Torr. (Bottom) Calculated spectrum with J values up to 15.

THEORY

The effective Hamiltonian for the vibrational interacting states $v_1 = 1/v_3 = 1/v_2 = 2/v_2 = v_4 = 1/v_4 = 2$ has been expressed in the tetrahedral tensorial formalism introduced in Ref. (*23*). A comprehensive account of the theory including relationship with other formulations (*5*) can be found in Refs. (*23, 24*). According to the vibrational extrapolation scheme (*24, 25*) the partially transformed vibration–rotation Hamiltonian adapted to the well-known vibrational pattern of methane can be written as

$$\mathscr{H} = \mathscr{H}_{\{GS\}} + \mathscr{H}_{\{Dyad\}} + \mathscr{H}_{\{Pentad\}} + \cdots . \tag{1}$$

In this expression $\mathscr{H}_{\{GS\}}$ contains only pure rotational operators of the type J^Ω (J designating one component J_x, J_y, or J_z of the angular momentum operator). In the notation introduced in Refs. (*23, 24*) its tensorial expression is

$$\mathscr{H}_{\{GS\}} = \sum t_0^{\Omega(K,A_1)} \mathbf{T}_0^{\Omega(K,A_1)}. \tag{2}$$

Similarly $\mathscr{H}_{\{Dyad\}}$ gathers all terms of type $r^2 J^\Omega$ (r designating the bending normal coordinates or conjugate momenta).

$$\mathscr{H}_{\{Dyad\}} = \sum t_{b_1,b_2}^{\Omega(K,\Gamma)\Gamma_1\Gamma_2} \mathbf{T}_{b_1,b_2}^{\Omega(K,\Gamma)\Gamma_1\Gamma_2} \tag{3}$$

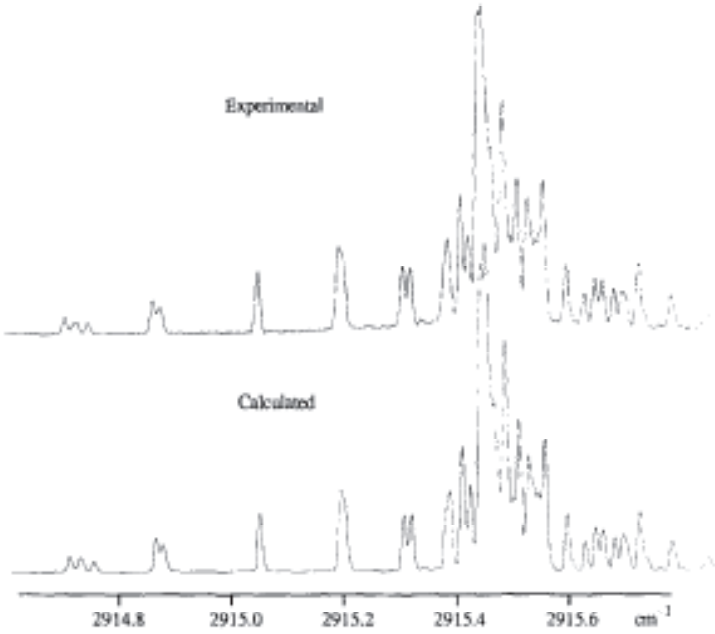

FIG. 4. Stimulated Raman spectrum of $^{13}CH_4$ (90% enriched). Scan c. (Top) Experimental spectrum using single pass cell with $T = 293$ K, $P = 3.3$ Torr. (Bottom) Calculated spectrum with J values up to 15. All lines arise from ν_1 transitions of $^{13}CH_4$ (see Table II).

with $b_1, b_2 = 2, 2$ or $2, 4$ or $4, 4$.

Finally, $\mathscr{H}_{\{\text{Pentad}\}}$ contains terms of three different types,

$$\mathscr{H}_{\{\text{Pentad}\}} = \sum t^{\Omega(K,\Gamma)\Gamma_1\Gamma_2}_{s_1,s_2}\mathbf{T}^{\Omega(K,\Gamma)\Gamma_1\Gamma_2}_{s_1,s_2} + \sum t^{\Omega(K,\Gamma)\Gamma_1\Gamma_2}_{s_1,b_1b_2}\mathbf{T}^{\Omega(K,\Gamma)\Gamma_1\Gamma_2}_{s_1,b_1b_2} + \sum t^{\Omega(K,\Gamma)\Gamma_1\Gamma_2}_{b_1b_2,b_3b_4}\mathbf{T}^{\Omega(K,\Gamma)\Gamma_1\Gamma_2}_{b_1b_2,b_3b_4} \quad (4)$$

where s_1 and s_2 designate one of the stretching modes ν_1 or ν_3 and b_1, b_2, b_3, b_4 one of the bending modes ν_2 and ν_4.

The first group in Eq. (4) contains r^2J^Ω terms relating to the stretching dyad ν_1/ν_3. The second group contains r^3J^Ω terms describing vibration–rotation interactions between the stretching dyad ν_1/ν_3 and the bending triad $2\nu_2/\nu_2 + \nu_4/2\nu_4$. The third group contains r^4J^Ω terms relating to the bending triad. Some of the latter terms can be regarded as vibrational corrections of terms involved in Eq. (3).

The effective Hamiltonian for the pentad upper states is defined by

$$\mathbf{H}^{\langle\text{Pentad}\rangle} = \mathbf{P}^{\langle\text{Pentad}\rangle}\mathscr{H}\mathbf{P}^{\langle\text{Pentad}\rangle}, \quad (5)$$

where $\mathbf{P}^{\langle\text{Pentad}\rangle}$ is the projector operator on the vibrational Hilbert subspace spanned by the pentad upper vibrational sublevels. According to the vibrational coupling scheme, the terms with nonvanishing matrix elements are organized into three groups,

$$\mathbf{H}^{\langle\text{Pentad}\rangle} = \mathbf{H}^{\langle\text{Pentad}\rangle}_{\{\text{GS}\}} + \mathbf{H}^{\langle\text{Pentad}\rangle}_{\{\text{Dyad}\}} + \mathbf{H}^{\langle\text{Pentad}\rangle}_{\{\text{Pentad}\}}. \quad (6)$$

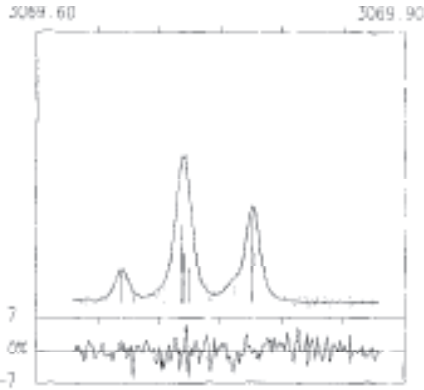

FIG. 5. Profile fitting example of the stimulated Raman spectrum of $^{13}CH_4$ (90% enriched, Scan b). T = 293 K, P = 36 Torr. Line positions of $^{13}CH_4$ transitions only were freely adjusted. Intensities and widths of $^{13}CH_4$ transitions were tied to predicted values, all line parameters of $^{12}CH_4$ (dotted ticks) were fixed. Residuals are expressed in percent of the strongest line of Fig. 3.

In this expression, subscripts refer to the operator type while superscripts refer to the subspace into which the operators contribute. The Hamiltonian parameters involved in the first two groups were already known from the ground state and dyad analyses through the corresponding $\mathbf{H}^{(GS)}$ and $\mathbf{H}^{(Dyad)}$ effective Hamiltonians. Thus only parameters included in $\mathscr{H}_{\{Pentad\}}$ had to be fitted to pentad data. To keep the number of adjustable parameters within reasonable bounds, the expansion was limited to the fourth order of approximation in the Amat Nielsen ordering scheme, whereas the first two parts of Eq. (6) were known up to the sixth order (*2*).

Table III shows the terms included in our model displayed as a function of their rotational degrees and according to Watson notation. It is noteworthy that the overall vibrational degeneracy of the problem is 19 and the number of terms in $\mathscr{H}^{(4)}_{\{Pentad\}}$ allowed by symmetry is 134. Consequently, on average, there are approximately seven parameters per vibrational degree of freedom. In addition, a reduced form of the transformed Hamiltonian contains much less adjustable parameters by removing essential correlations among parameters (*26*). Combined with the vibrational extrapolation scheme, remaining correlations are minimized further, for instance, since the adjusted terms from $\mathscr{H}^{(4)}_{\{Pentad\}}$ have relatively low J dependences: up to J^4 for the stretching dyad, up to J^3 for stretch–bend interaction terms, and up to J^2 only for the bending overtone and combination bands. However in the present preliminary work, only the lower-order ambiguities have been removed, whereas all fourth-order parameters have been damped in order to ensure the convergence of the least-squares fit.

RESULTS AND DISCUSSION

A series of programs written in FORTRAN and adapted to the SUN 4 workstations at Dijon was used to refine the upper state parameters from $\mathscr{H}_{\{Pentad\}}$ to fit infrared and Raman data simultaneously. In the least-squares procedure, the weights of the

data were set proportional to the inverse of their estimated variances so that the weighted residuals can be considered as centered (expectation value = zero) and reduced (variance = unity) random variables. In this preliminary study the model accuracy was taken into account in a crude way. The values used to weight the data (10^{-3} cm^{-1} for infrared, $1-2 \times 10^{-3}$ cm^{-1} for Raman) were intended to account uniformly for both experimental precision and model accuracy. The latter was assumed to be independent of any quantum numbers.

The assignment and analysis were achieved progressively starting from predictions using known or estimated values of Hamiltonian parameters. In addition to the well-determined parameters from $\mathscr{H}_{\{GS\}}$ and $\mathscr{H}_{\{Dyad\}}$ (*1, 2*), we used an initial set of $\mathscr{H}_{\{Pentad\}}$ parameters derived from those of $^{12}CH_4$ by shifting the ν_3 band center according to values of isolated ν_3 band analyses (*10–12*). This initial prediction allowed most of the strongest features of the infrared spectra to be assigned. Similarly, the assigned ν_1 Raman transitions (Table II) were included in the fit. Progressively, most of the upper levels of all five bands were reached by at least one infrared or Raman assigned transition up to J equal 10 (see energy diagrams on Fig. 6). According to the methodology applied in Ref. (*2*), the assignment/selection process of the experimental infrared data was done iteratively in two steps. (i) The line positions were predicted and matched with observed line centers automatically by computer. (ii) The final selection for inclusion in the fit was done manually after meticulous inspection of the plotted spectra in order to eliminate suspicious blends. At no time was the choice of good candidates for the fit based on the current observed minus calculated residuals.

Table II gives the results of the fitting for Raman data, showing its measured positions, assumed weight, assignment, obs.-calc. standard deviation, and relative intensity. As in the other recent polyad studies (*1–4*), the assignment notation for the polyad levels listed in Table II is given by three quantum numbers, J, C, α, rather than five, J, R, C, n, v (vibrational id), used for the isolated band studies of triply degenerate fundamentals and other bands presenting similar patterns. The groups of levels previously designated by R, n, and v at each symmetry C (A_1, A_2, E, F_1, F_2) of each J are now indexed together using α. Starting with those of $2\nu_4$, the pentad levels are counted in order of ascending values of energy without distinguishing the vibrational identity. Thus in Table II, the α values for the ν_3 transitions are rather high values. However, for modest J, the conversion to the old notation may be straightforward, if one knows the number and energies of the rotational levels associated with each pentad vibrational degeneracy. For example, in Table II the Raman transition at 3967.3627 cm^{-1} is 5 E 1 to 6 E 15 of ν_3; for $J = 6$, there are seven E levels of $2\nu_4$ ($\alpha = 1-7$), six E levels of $\nu_2 + \nu_4$ ($\alpha = 8-13$), and one E level of ν_1 ($\alpha = 14$) with upper state energies lower than this one of ν_3 ($\alpha = 15$). The 6 E 15 level corresponds to 6 5 E 1 in the older notation; it gives rise to a strong $R(-)$ transition in the infrared. Similarly, the Raman transition at 3069.5486 cm^{-1} is R 5 E 1 to 6 E 16; in isolated band notation, this is the 6 6 E 1 level which gives rise to an allowed $Q(0)$ infrared line. These notational changes do not alter the principal transition selections rules of $\Delta J = 0, \pm 1$ with $\Delta C = 0$ for Raman and $\Delta C \neq 0$ for infrared, but the designation of allowed ($\Delta R = 0$ and $\Delta n = 0$) and forbidden ($\Delta R \neq 0$ or $\Delta n \neq 0$) (relevant for weakly perturbed states of triply degenerate bands) is lost in the present scheme (especially designed to account for any kind of strongly perturbed states). For clarity, the vibra-

TABLE II

Line Position Measurements of the Raman Spectrum of $^{13}CH_4$

Measured[a] cm^{-1}		Precision[b] cm^{-1}	Assignment J_0 C_0 α_0							vib[c]		Obs-Cal cm^{-1}	St.Dev[d] cm^{-1}	Intensity[e] a.u.
a	3063.9640	+	0.0020	Q	0	A1	1	0	A1	3	2v2	A1	100%	0.0019	0.0002	0.342E-03
a	3064.2874	+	0.0010	Q	1	F1	1	1	F1	8	2v2	A1	99%	0.0013	0.0002	0.569E-03
a	3064.8193	+	0.0010	Q	2	E	1	2	E	8	2v2	A1	92%	-0.0001	0.0002	0.512E-03
a	3064.8851	+	0.0010	Q	2	F2	1	2	F2	12	2v2	A1	95%	-0.0002	0.0002	0.789E-03
a	3065.4555	+	0.0010	Q	3	F1	1	3	F1	16	2v2	A1	81%	-0.0003	0.0001	0.776E-03
b	3065.4566	+	0.0010	Q	3	F1	1	3	F1	16	2v2	A1	81%	0.0009	0.0001	0.776E-03
a	3065.6318	+	0.0010	Q	3	F2	1	3	F2	14	2v2	A1	84%	-0.0004	0.0001	0.797E-03
b	3065.6328	+	0.0010	Q	3	F2	1	3	F2	14	2v2	A1	84%	0.0006	0.0001	0.796E-03
b	3065.9679	+	0.0005	Q	3	A2	1	3	A2	7	2v2	A1	99%	0.0004	0.0002	0.153E-02
a	3065.9681	+	0.0005	Q	3	A2	1	3	A2	7	2v2	A1	99%	0.0006	0.0002	0.153E-02
b	3066.0783	+	0.0005	Q	4	A1	1	4	A1	8	2v2	A1	72%	-0.0009	0.0001	0.115E-02
a	3066.0792	+	0.0005	Q	4	A1	1	4	A1	8	2v2	A1	72%	0.0000	0.0001	0.115E-02
b	3066.2262	+	0.0010	Q	4	F1	1	4	F1	18	2v2	A1	71%	-0.0006	0.0001	0.680E-03
a	3066.2267	+	0.0010	Q	4	F1	1	4	F1	18	2v2	A1	71%	-0.0001	0.0001	0.680E-03
b	3066.3309	+	0.0010	Q	4	E	1	4	E	13	2v2	A1	71%	-0.0007	0.0001	0.446E-03
a	3066.3315	+	0.0010	Q	4	E	1	4	E	13	2v2	A1	71%	-0.0002	0.0001	0.446E-03
b	3066.5440	-	0.0050	Q	2	F2	1	2	F2	13	2v2	E	95%	-0.0008	0.0003	0.335E-04
b	3066.6780	-	0.0050	Q	2	E	1	2	E	9	2v2	E	92%	-0.0067	0.0003	0.364E-04
b	3066.9228	+	0.0010	Q	5	F1	1	5	F1	24	2v2	A1	66%	0.0005	0.0001	0.535E-03
b	3067.0507	+	0.0015	Q	5	F2	1	5	F2	22	2v2	A1	63%	0.0006	0.0001	0.801E-03
b	3067.0678	+	0.0010	Q	4	F2	1	4	F2	20	2v2	A1	88%	0.0005	0.0001	0.990E-03
b	3067.3569	-	0.0050	R	5	F2	1	6	F2	23	v3	F2	92%	0.0015	0.0002	0.148E-03
b	3067.3627	-	0.0050	R	5	E	1	6	E	15	v3	F2	92%	0.0009	0.0002	0.693E-04
b	3067.4319	-	0.0050	Q	3	F2	1	3	F2	15	2v2	E	96%	0.0007	0.0003	0.289E-04
b	3067.4465	-	0.0050	R	5	F1	2	6	F1	21	v3	F2	92%	0.0012	0.0002	0.175E-03
b	3067.7796	+	0.0015	Q	6	E	1	6	E	18	2v2	A1	61%	0.0002	0.0001	0.285E-03
b	3067.8107	+	0.0010	Q	6	F2	1	6	F2	28	2v2	A1	60%	0.0004	0.0001	0.416E-03
b	3067.8620	+	0.0050	Q	3	F2	1	3	F2	16	2v2	E	87%	-0.0003	0.0002	0.951E-04
b	3067.8798	+	0.0010	Q	6	A2	1	6	A2	9	2v2	A1	57%	0.0002	0.0001	0.666E-03
b	3068.1202	+	0.0020	Q	3	F1	1	3	F1	18	2v2	E	80%	0.0006	0.0002	0.147E-03
b	3068.2301	+	0.0010	Q	5	E	1	5	E	16	2v2	A1	78%	-0.0004	0.0001	0.413E-03
b	3068.3749	+	0.0010	Q	5	F1	2	5	F1	25	2v2	A1	77%	-0.0005	0.0001	0.605E-03
b	3068.7098	+	0.0010	Q	7	F1	1	7	F1	32	2v2	A1	58%	0.0003	0.0002	0.305E-03
b	3068.7346	+	0.0010	Q	7	F2	1	7	F2	30	2v2	A1	56%	0.0002	0.0002	0.293E-03
b	3069.3990	+	0.0040	Q	4	F2	1	4	F2	22	2v2	E	88%	-0.0002	0.0002	0.880E-04
b	3069.5104	+	0.0010	Q	6	F2	2	6	F2	29	2v2	A1	71%	-0.0003	0.0001	0.435E-03
b	3069.5486	-	0.0050	R	5	E	1	6	E	16	v3	F2	91%	-0.0002	0.0002	0.393E-03
b	3069.5763	-	0.0050	R	5	F1	2	6	F1	22	v3	F2	91%	-0.0002	0.0002	0.387E-03
b	3069.5926	-	0.0050	R	5	F1	1	6	F1	22	v3	F2	91%	0.0015	0.0002	0.613E-04
b	3069.6696	+	0.0030	Q	4	E	1	4	E	15	2v2	E	71%	-0.0007	0.0002	0.136E-03
b	3069.7181	-	0.0050	Q	8	F1	1	8	F1	34	2v2	A1	55%	-0.0022	0.0002	0.343E-03
b	3069.7198	-	0.0050	Q	8	A1	1	8	A1	13	2v2	A1	56%	0.0038	0.0002	0.202E-03
b	3069.7230	-	0.0050	Q	8	E	1	8	E	24	2v2	A1	54%	0.0008	0.0002	0.134E-03
b	3069.7763	+	0.0010	Q	6	F1	1	6	F1	26	2v2	A1	68%	-0.0007	0.0001	0.420E-03
b	3070.0501	+	0.0020	Q	4	F1	1	4	F1	20	2v2	E	72%	-0.0005	0.0002	0.188E-03
b	3070.1490	+	0.0010	Q	6	A1	1	6	A1	11	2v2	A1	68%	-0.0012	0.0001	0.691E-03
b	3070.2470	-	0.0050	R	5	F1	2	6	F1	23	v3	F2	91%	0.0004	0.0001	0.281E-03
c	2914.7083	+	0.0010	Q	11	F2	1	11	F2	35	v1	A1	80%	0.0004	0.0003	0.720E-01
c	2914.7088	+	0.0010	Q	12	E	1	12	E	26	v1	A1	75%	-0.0020	0.0004	0.264E-01
c	2914.7229	-	0.0050	Q	12	F1	1	12	F1	38	v1	A1	75%	-0.0008	0.0004	0.401E-01
c	2914.7309	+	0.0010	Q	11	F1	1	11	F1	36	v1	A1	80%	0.0013	0.0003	0.621E-01
c	2914.7491	+	0.0010	Q	12	A1	1	12	A1	14	v1	A1	75%	-0.0019	0.0004	0.651E-01
c	2914.8636	+	0.0010	Q	10	A2	1	10	A2	11	v1	A1	83%	0.0008	0.0002	0.201E+00
c	2914.8744	+	0.0010	Q	10	F2	1	10	F2	33	v1	A1	83%	0.0007	0.0002	0.115E+00
c	2914.8798	+	0.0010	Q	10	E	1	10	E	22	v1	A1	83%	0.0007	0.0002	0.858E-01
c	2915.0494	+	0.0010	Q	9	F2	1	9	F2	29	v1	A1	84%	0.0014	0.0002	0.173E+00
c	2915.0502	+	0.0010	Q	9	F1	1	9	F1	30	v1	A1	84%	0.0015	0.0002	0.178E+00
c	2915.1931	+	0.0010	Q	8	A1	1	8	A1	10	v1	A1	86%	0.0012	0.0002	0.434E+00
c	2915.2003	+	0.0010	Q	8	F1	1	8	F1	26	v1	A1	86%	0.0010	0.0002	0.280E+00
c	2915.2047	-	0.0050	Q	8	E	1	8	E	18	v1	A1	86%	0.0015	0.0002	0.203E+00
c	2915.3079	+	0.0010	Q	7	F1	1	7	F1	24	v1	A1	87%	0.0011	0.0002	0.311E+00
c	2915.3210	+	0.0010	Q	7	F2	1	7	F2	23	v1	A1	87%	0.0007	0.0002	0.295E+00
c	2915.3815	+	0.0010	Q	6	E	1	6	E	14	v1	A1	87%	-0.0001	0.0002	0.281E+00

(a) Wavenumbers obtained by profile fitting. Preceding letters refer to scans.
+ signs designate transitions included in the refinement of Hamiltonian parameters.
(b) Quality factor derived from profile fitting statistics.
(c) Main vibrational components deduced from eigenvector analysis.
(d) Calculated from the variance matrix of Hamiltonian parameters.
(e) Zeroth order calculated relative intensity.

TABLE II—*Continued*

Measured[a] cm^{-1}	Precision[b] cm^{-1}	Assignment J_0 C_0 n_0	Assignment J C n	vib[c]	Obs-Cal cm^{-1}	St.Dev[d] cm^{-1}	Intensity[e] a.u.
c 2915.3894 +	0.0010	Q 6 F2 1	6 F2 21	v1 A1	87% 0.0001	0.0002	0.427E+00
c 2915.4113 +	0.0010	Q 6 A2 1	6 A2 7	v1 A1	87% 0.0002	0.0002	0.697E+00
c 2915.4249 +	0.0010	Q 5 F1 1	5 F1 18	v1 A1	88% -0.0004	0.0003	0.480E+00
c 2915.4408 -	0.0050	Q 4 A1 1	4 A1 6	v1 A1	89% -0.0016	0.0004	0.947E+00
c 2915.4426 -	0.0050	Q 0 A1 1	0 A1 2	v1 A1	90% 0.0002	0.0007	0.174E+00
c 2915.4426 -	0.0050	Q 5 F2 1	5 F2 17	v1 A1	88% -0.0023	0.0003	0.536E+00
c 2915.4454 -	0.0050	Q 1 F1 1	1 F1 6	v1 A1	90% -0.0006	0.0007	0.307E+00
c 2915.4491 -	0.0050	Q 2 E 1	2 E 6	v1 A1	90% -0.0019	0.0006	0.293E+00
c 2915.4499 -	0.0050	Q11 E 1	11 E 24	v1 A1	79% -0.0013	0.0002	0.451E-01
c 2915.4502 -	0.0050	Q 4 F1 1	4 F1 14	v1 A1	89% -0.0035	0.0004	0.557E+00
c 2915.4516 -	0.0050	Q 2 F2 1	2 F2 9	v1 A1	90% -0.0012	0.0006	0.429E+00
c 2915.4526 -	0.0050	Q 3 F1 1	3 F1 12	v1 A1	89% -0.0014	0.0005	0.511E+00
c 2915.4587 -	0.0050	Q 3 F2 1	3 F2 11	v1 A1	89% -0.0022	0.0005	0.555E+00
c 2915.4588 -	0.0050	Q 4 E 1	4 E 10	v1 A1	89% -0.0029	0.0004	0.379E+00
c 2915.4673 +	0.0020	Q 3 A2 1	3 A2 5	v1 A1	89% -0.0025	0.0005	0.100E+01
c 2915.4761 -	0.0050	Q10 F1 1	10 F1 32	v1 A1	81% 0.0009	0.0002	0.110E+00
c 2915.4820 -	0.0050	Q 9 E 1	9 E 20	v1 A1	83% 0.0006	0.0002	0.127E+00
c 2915.4820 -	0.0050	Q10 F2 2	10 F2 34	v1 A1	81% 0.0025	0.0002	0.123E+00
c 2915.4849 +	0.0020	Q 7 A2 1	7 A2 9	v1 A1	86% -0.0021	0.0002	0.668E+00
c 2915.4865 -	0.0050	Q11 F2 2	11 F2 36	v1 A1	78% 0.0028	0.0002	0.667E-01
c 2915.4882 +	0.0020	Q 4 F2 1	4 F2 15	v1 A1	89% 0.0011	0.0004	0.623E+00
c 2915.4913 -	0.0050	Q 8 F2 1	8 F2 27	v1 A1	85% 0.0002	0.0002	0.285E+00
c 2915.4957 -	0.0050	Q 9 F1 2	9 F1 31	v1 A1	83% 0.0013	0.0002	0.197E+00
c 2915.5012 -	0.0050	Q 5 E 1	5 E 12	v1 A1	88% -0.0010	0.0003	0.413E+00
c 2915.5040 -	0.0050	Q12 F1 2	12 F1 39	v1 A1	75% 0.0019	0.0003	0.378E-01
c 2915.5106 +	0.0020	Q 5 F1 2	5 F1 19	v1 A1	88% -0.0013	0.0003	0.590E+00
c 2915.5137 +	0.0020	Q 6 F2 2	6 F2 22	v1 A1	87% -0.0003	0.0002	0.499E+00
c 2915.5288 -	0.0050	Q 7 F2 2	7 F2 24	v1 A1	86% 0.0002	0.0002	0.420E+00
c 2915.5291 -	0.0050	Q 9 A1 1	9 A1 10	v1 A1	83% -0.0006	0.0002	0.357E+00
c 2915.5370 -	0.0050	Q 6 F1 1	6 F1 20	v1 A1	87% -0.0007	0.0002	0.496E+00
c 2915.5448 -	0.0050	Q 8 F1 2	8 F1 27	v1 A1	85% -0.0011	0.0002	0.353E+00
c 2915.5500 -	0.0050	Q 7 E 1	7 E 16	v1 A1	86% -0.0034	0.0002	0.234E+00
c 2915.5519 -	0.0050	Q11 A2 1	11 A2 13	v1 A1	77% 0.0049	0.0003	0.117E+00
c 2915.5586 +	0.0010	Q 6 A1 1	6 A1 8	v1 A1	87% -0.0010	0.0002	0.941E+00
c 2915.5691 -	0.0050	Q13 F2 3	13 F2 41	v1 A1	70% -0.0014	0.0005	0.173E-01
c 2915.5983 +	0.0010	Q 7 F1 2	7 F1 25	v1 A1	86% -0.0005	0.0002	0.360E+00
c 2915.6115 -	0.0050	Q12 F2 1	12 F2 39	v1 A1	74% 0.0018	0.0003	0.374E-01
c 2915.6306 +	0.0010	Q 8 E 2	8 E 19	v1 A1	84% -0.0005	0.0002	0.186E+00
c 2915.6496 +	0.0010	Q 8 F2 2	8 F2 28	v1 A1	84% -0.0006	0.0002	0.264E+00
c 2915.6624 -	0.0050	Q 9 F1 3	9 F1 32	v1 A1	83% -0.0010	0.0002	0.191E+00
c 2915.6643 -	0.0050	Q12 A2 1	12 A2 13	v1 A1	76% 0.0010	0.0004	0.706E-01
c 2915.6828 +	0.0010	Q10 A1 1	10 A1 12	v1 A1	80% -0.0011	0.0002	0.203E+00
c 2915.6969 +	0.0020	Q 9 F2 2	9 F2 30	v1 A1	83% -0.0010	0.0003	0.174E+00
c 2915.7045 -	0.0050	Q13 A1 1	13 A1 14	v1 A1	69% 0.0001	0.0005	0.342E-01
c 2915.7054 +	0.0020	Q10 F1 2	10 F1 33	v1 A1	80% -0.0004	0.0003	0.100E+00
c 2915.7267 +	0.0010	Q 9 A2 1	9 A2 11	v1 A1	82% -0.0011	0.0003	0.305E+00
c 2915.7305 -	0.0050	Q10 E 2	10 E 23	v1 A1	81% 0.0001	0.0003	0.748E-01
c 2915.7403 +	0.0020	Q11 F2 3	11 F2 37	v1 A1	78% 0.0003	0.0003	0.548E-01
c 2915.7836 -	0.0050	Q10 F2 3	10 F2 35	v1 A1	80% -0.0011	0.0003	0.855E-01
c 2915.7894 -	0.0050	Q11 F1 2	11 F1 37	v1 A1	77% -0.0003	0.0003	0.539E-01
c 2915.8431 +	0.0010	Q11 E 2	11 E 25	v1 A1	78% -0.0006	0.0003	0.343E-01
c 2915.8517 +	0.0010	Q11 F1 3	11 F1 38	v1 A1	78% -0.0011	0.0003	0.485E-01

tional assignments are also shown in Table II. These are based on the eigenvector analysis. As in Ref. (*2*), the calculated percentages correspond to the projection of the upper state eigenvector onto its major vibrational component: percentages close to 100% refer to vibrationally pure eigenstates whereas smaller percentages characterize heavy vibrational hybridation.

The agreement achieved between theory and experiment is illustrated in Fig. 7. Observed − calculated frequencies are displayed as a function of J and separately for the five bands. No pronounced dependence of the quality of the analysis with vibrational or rotational quantum numbers is observed. Also at the present stage no inconsistency

TABLE III

Partially Transformed Hamiltonian

Rotational Degree		Bending Dyad	Stretching / Bending Dyad Triad
0	-	H_{20}	$H_{20} + H_{30} + H_{40}$ [a]
1	-	H_{21}	$H_{21} + H_{31} + H_{41}$
2	H_{02}	H_{22}	$H_{22} + H_{32} + H_{42}$
3	-	H_{23}	$H_{23} + H_{33}$
4	H_{04}	H_{24}	H_{24}
5	-	H_{25}	
6	H_{06}	H_{26}	
7	-		
8	H_{08}		

$$\mathfrak{H} = \mathfrak{H}^{(6)}_{[G.S.]} + \mathfrak{H}^{(6)}_{[Dyad]} + \mathfrak{H}^{(4)}_{[Pentad]} + \cdots$$

Vib Degeneracy	1	+	5	+	19	=	25
Nb parameters[b]	10	+	62	+	134	=	206
$\frac{\text{Nb parameters}}{\text{Vib Degeneracy}}$	**10**	=	**12**	=	**7**	=	**8**

(a) H_{nm} refers to Watson classification scheme.

(b) Numbers quoted correspond to all parameters allowed by symmetry.

of absolute position measurements from the different sources of experimental data can be detected: the distributions of residuals from Raman or infrared data appear both centered on the zero axis. These preliminary results represent already an improvement with respect to the study of the same band system of the $^{12}CH_4$ molecule published in Refs. (*3, 4*). The standard deviation of the fit was of the order of 20×10^{-3} cm^{-1} as compared with the present values of 0.71×10^{-3} cm^{-1} for infrared data, 0.93×10^{-3} cm^{-1} for the ν_1 Raman data, and 0.64×10^{-3} cm^{-1} for the $2\nu_2$ Raman data. In addition, the $^{12}CH_4$ data from Refs. (*3, 4*) have also been refitted with a similar result. The primary reason for such an improvement has been the extension of the Hamiltonian model to fourth order. Table IV shows selected sets of Hamiltonian parameters from $\mathscr{H}_{[\text{Pentad}]}$. It is interesting to see the individual sensitivity of the parameters to the different sources of experimental data. A relevant quantity for this is the percentage contributions as introduced in Ref. (*27*). One can see the quantitative confirmation of the importance of the ν_1 Raman transitions for the determination of the lower-order "ν_1-parameters." The same conclusion applies for the $2\nu_2$ Raman transitions, to a lesser extent because a substantial number of $2\nu_2$ infrared transitions allowed by perturbation are already included in the fit. Toward higher J values, since

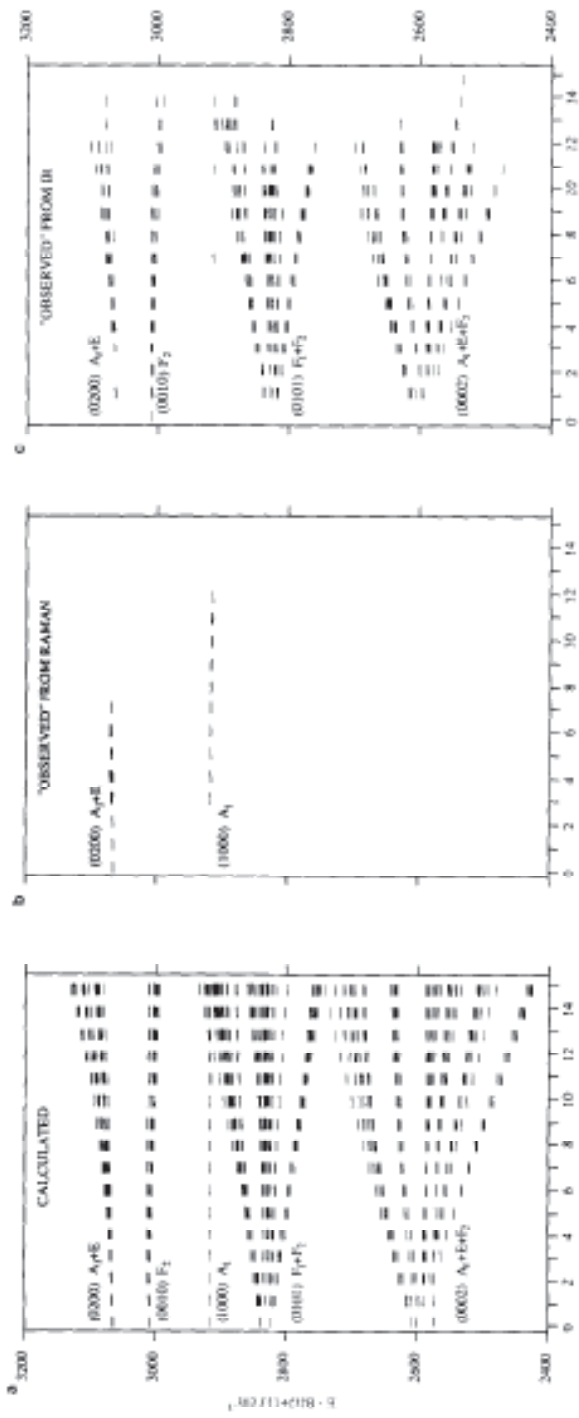

FIG. 6. Schematic energy diagram of the upper states of the pentad of $^{13}CH_4$. (a) Calculated energy levels from $J = 0$ through 15. (b) Energy levels reached by at least one Raman transition included in the fit. (c) Energy levels reached by at least one infrared transition included in the fit.

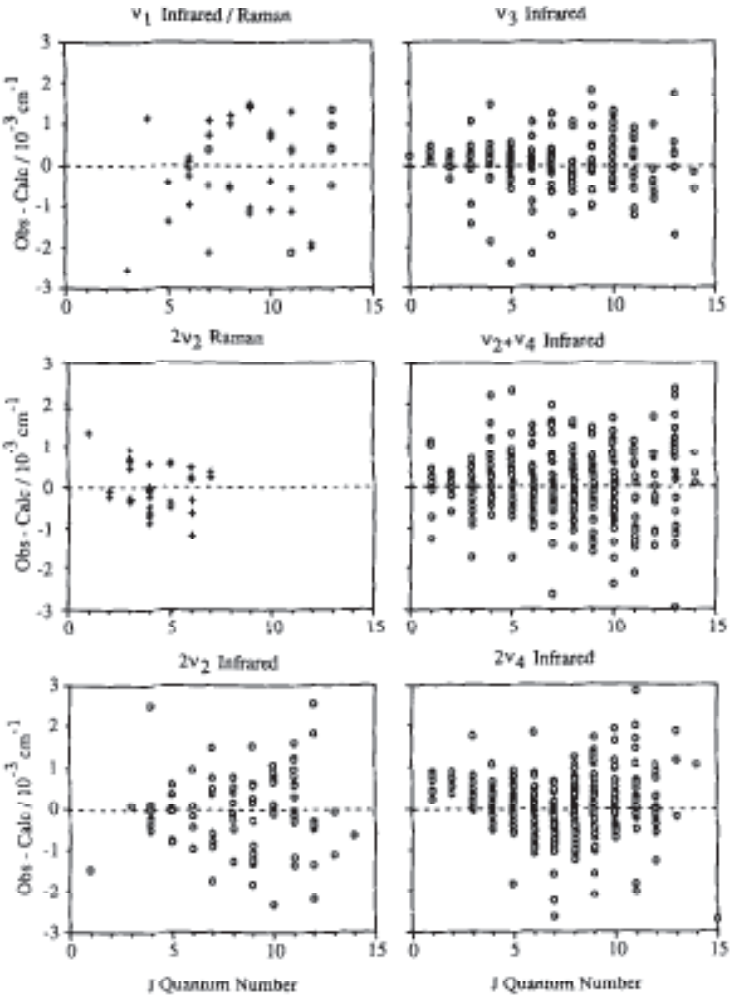

FIG. 7. Observed − calculated versus J for $^{13}CH_4$. (○) All fitted IR transitions; (+) all fitted Raman transitions.

interaction effects are increasing, more and more infrared "forbidden" transitions become observable and assignable so that infrared data play an increasing role in the determination of higher-order parameters for all bands. The degrees of freedom quoted in Table IV indicate to what extent a given parameter value is depending upon the other parameters. It ranges from the value 0 (complete dependence with respect to other parameters) to the value 1 (complete independence, i.e., complete freedom). Within these theoretical limits, the degree of freedom is a decreasing function of the number of fitted parameters and of their mutual correlations.

The present quality of the results is indicated by a direct comparison of observed and synthetic spectra in the region of the ν_3 Q branch. Figure 8 shows the apodized infrared spectrum from 3002 to 3012 cm^{-1} with the obs.-calc. residuals plotted below.

TABLE IV

Selected Hamiltonian Parameters for $^{13}CH_4$

Parameter			Value(StDev) cm^{-1}	Frdm [a] x1000	From [b] A	B	C
	ν_1						
0(0,0A1)	A1	H20	2882.3414(12)	131	16.8	83.2	0.0
2(0,0A1)	A1	H22	-4.3725(45) 10^{-2}	34	36.6	63.4	0.0
4(0,0A1)	A1	H24	1.708(27) 10^{-5}	40	56.0	44.0	0.0
4(4,0A1)	A1	H24	-2.794(37) 10^{-6}	111	29.6	69.4	0.0
	$\nu_1 - \nu_3$						
2(2,0F2)	A1-F2	H22	-4.888(27) 10^{-2}	29	98.7	1.3	0.0
4(2,0F2)	A1-F2	H24	-3.87(16) 10^{-6}	127	98.3	0.7	0.0
4(4,0F2)	A1-F2	H24	-7.72(84) 10^{-7}	422	98.3	0.7	0.0
	$\nu_1 - 2\nu_2$						
2(0,0A1)	A1-A1	H32	2.921(43) 10^{-3}	108	83.3	15.6	0.2
2(2,0E)	A1-E	H32	8.060(92) 10^{-3}	59	58.1	41.8	0.2
	$\nu_1 - \nu_2+\nu_4$						
1(1,0F1)	A1-F1	H31	-5.163(91) 10^{-2}	37	70.7	29.3	0.0
3(1,0F1)	A1-F1	H33	1.35(99) 10^{-6}	107	78.5	20.5	0.0
3(3,0F1)	A1-F1	H33	3.57(15) 10^{-5}	107	88.3	10.7	0.0
2(2,0F2)	A1-F2	H32	-5.04(10) 10^{-3}	24	92.0	8.0	0.0
3(3,0F2)	A1-F2	H33	1.997(18) 10^{-4}	128	91.6	7.4	0.0
	$2\nu_2$						
0(0,0A1)	A1	H40	-3.38465(87)	145	29.3	0.0	70.7
2(0,0A1)	A1	H42	-2.672(21) 10^{-3}	110	87.3	0.0	11.7
2(2,0E)	A1-E	H42	-8.961(91) 10^{-4}	171	86.9	0.0	12.1
0(0,0A1)	E	H40	-1.32440(33)	326	94.3	0.0	5.7
2(0,0A1)	E	H42	-2.176(10) 10^{-3}	116	98.2	0.0	0.8
2(2,0E)	E	H42	-4.80(17) 10^{-4}	169	96.0	0.0	3.0
	$2\nu_2 - 2\nu_4$						
0(0,0A1)	A1-A1	H40	-8.041(44)	39	73.6	17.7	8.7
2(0,0A1)	A1-A1	H42	1.3466(90) 10^{-2}	133	84.5	14.2	0.3
2(2,0E)	A1-E	H42	3.477(67) 10^{-3}	127	98.8	0.2	0.0
2(2,0F2)	A1-F2	H42	9.64(11) 10^{-3}	141	98.8	0.2	0.0
2(2,0E)	E-A1	H42	1.73(10) 10^{-3}	136	63.8	35.0	0.2

FITTED DATA

A	1148 IR transitions	Jmax 15	R.M.S.	0.000 71 cm^{-1}
B	33 Raman transitions (ν_1)	Jmax 13	R.M.S.	0.000 93 cm^{-1}
C	34 Raman transitions ($2\nu_2$)	Jmax 8	R.M.S.	0.000 64 cm^{-1}

(a) Degree of freedom with respect to all other parameters adjusted (see Text).

(b) Percentage contribution of the three sets of data for the determination of the parameter.

The dominant transitions are the allowed $Q(0)$ branch up through $J = 14$ while the weaker transitions at the right belong to the forbidden $Q(+)$. The manifolds are satisfactorily reproduced in both branches for the transitions already included in the fit. However, extrapolating the prediction to even higher J gives poorer result. The agreement on the ν_1 Raman spectrum is also satisfactory (Fig. 4). In this case a direct comparison is impeded by heavy crowded features for which baseline, intensity, and profile inaccuracies produce drastic effects on the synthetic curve. However, the spectra

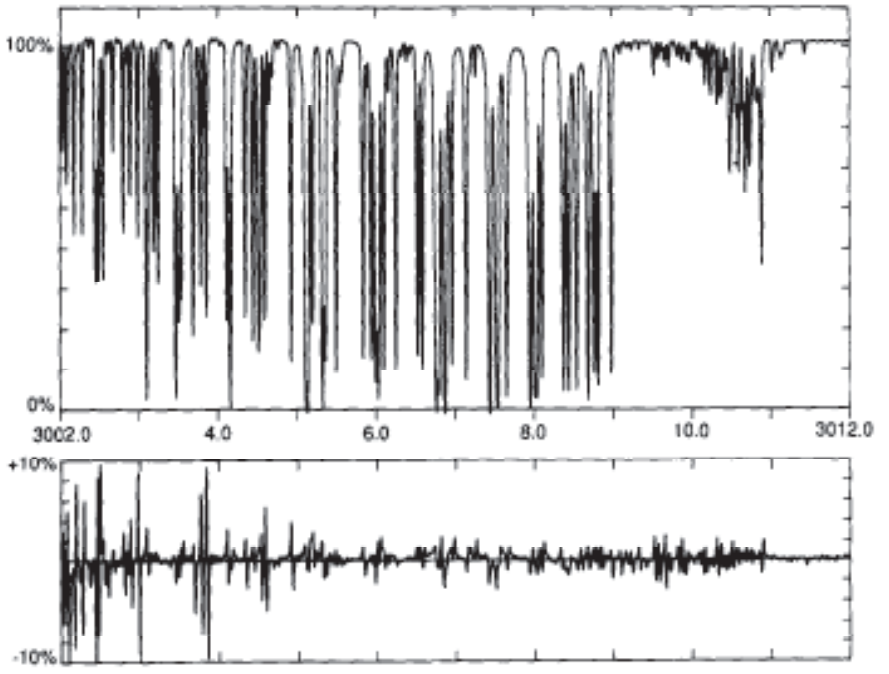

FIG. 8. The comparison of observed and calculated spectra using the infrared spectrum shown in Fig. 1. The effective resolution of the apodized spectrum is 0.016 cm^{-1}. The obs.-calc. residuals in percent are plotted in the panel below; the calculated spectrum is not plotted.

plotted in Figs. 2–4 show a satisfactory agreement between observed and synthesized traces probing a good agreement on line positions. Table II gives the individual standard deviations of calculated Raman transitions derived from the variance matrix of the Hamiltonian parameters. These values reflect the propagation of parameter uncertainties into predicted frequencies.

The complete study of the pentad system of both $^{12}CH_4$ and $^{13}CH_4$ isotopic species is in progress and will be reported in due course. To include higher J value observations it will be necessary to take into account the accuracy of the Hamiltonian model. Both vibrational and rotational dependences will have to be considered in order to get parameters capable of reproducing the observed spectra and reliable for predicting line positions with precisions estimated rigorously. Similarly, a detailed analysis of intensities to determine the dipole moment parameters is required to predict the pentad spectrum accurately. For the present, this preliminary analysis provides a useful prediction for identifying isolated transitions in the $^{13}CH_4$ spectrum and culling blended lines from consideration in the ongoing analyses.

ACKNOWLEDGMENT

The calculations of the present work have been made using laboratory computer equipment partly supported by Le Conseil Régional de Bourgogne.

RECEIVED: July 15, 1991

REFERENCES

1. J. P. Champion, J. C. Hilico, and L. R. Brown, *J. Mol. Spectrosc.* **133,** 244–255 (1989).
2. J. P. Champion, J. C. Hilico, C. Wenger, and L. R. Brown, *J. Mol. Spectrosc.* **133,** 256–272 (1989).
3. G. Poussigue, E. Pascaud, J. P. Champion, and G. Pierre, *J. Mol. Spectrosc.* **93,** 351–380 (1982).
4. G. Pierre, J. P. Champion, G. Guelachvili, E. Pascaud, and G. Poussigue, *J. Mol. Spectrosc.* **102,** 344–360 (1983).
5. J. E. Lolck and A. G. Robiette, *J. Mol. Spectrosc.* **88,** 14–29 (1981).
6. J. E. Lolck, A. G. Robiette, L. R. Brown, and R. H. Hunt, *J. Mol. Spectrosc.* **92,** 229–245 (1982).
7. H. Frunder, D. Illig, H. Finsterholzl, H. W. Schrotter, B. Lavorel, G. Roussel, J. C. Hilico, J. P. Champion, G. Pierre, G. Poussigue, and E. Pascaud, *Chem. Phys. Lett.* **100,** 110–114 (1983).
8. L. S. Rothman, *Appl. Opt.* **22,** 2247–2256 (1982).
9. R. A. Toth, L. R. Brown, R. H. Hunt, and L. S. Rothman, *Appl. Opt.* **20,** 932–935 (1981).
10. L. W. Pinkley, K. Narahari Rao, M. Dang-Nhu, G. Tarrago, and G. Poussigue, *J. Mol. Spectrosc.* **63,** 402–444 (1976).
11. M. Dang-Nhu, A. S. Pine, and A. G. Robiette, *J. Mol. Spectrosc.* **77,** 57–68 (1979).
12. R. S. McDowell, C. W. Patterson, and A. Owyoung, *J. Chem. Phys.* **72,** 1071–1076 (1980).
13. J. E. Lolck, G. Poussigue, E. Pascaud, and G. Guelachvili, *J. Mol. Spectrosc.* **111,** 235–274 (1985).
14. G. Millot, B. Lavorel, R. Chaux, R. Saint-Loup, G. Pierre, H. Berger, J. I. Steinfeld, and B. Foy, *J. Mol. Spectrosc.* **127,** 156–177 (1988).
15. D. E. Jennings, R. Hubbard, and J. W. Brault, *Appl. Opt.* **24,** 3438 (1985).
16. C. R. Pollock, F. R. Petersen, D. A. Jennings, J. S. Wells, and A. Maki, *J. Mol. Spectrosc.* **99,** 357–368 (1983).
17. V. Malathy Devi, D. C. Benner, M. A. H. Smith, and C. P. Rinsland, *Appl. Opt.* **30,** 287–304 (1991).
18. R. Saint-Loup, B. Lavorel, G. Millot, C. Wenger, and H. Berger, *J. Raman Spectrosc.* **21,** 77–83 (1990).
19. R. Chaux, C. Milan, G. Millot, B. Lavorel, R. Saint-Loup, and J. Moret-Bailly, *J. Opt. (Paris)* **19,** 3–14 (1988).
20. G. Guelachvili, *J. Mol. Spectrosc.* **75,** 251–269 (1979).
21. A. Boutahar, G. Millot, M. Loete, B. Lavorel, and C. Wenger, in preparation.
22. A. Boutahar and M. Loete, *Can. J. Phys.* **69,** 26–35 (1991).
23. J. P. Champion, *Can. J. Phys.* **55,** 1802–1828 (1977).
24. J. P. Champion and G. Pierre, *J. Mol. Spectrosc.* **79,** 255–280 (1980).
25. V. G. Tyuterev, J. P. Champion, and G. Pierre, *Mol. Phys.* **71,** 995–1020 (1990).
26. V. I. Perevalov, V. G. Tyuterev, and B. I. Zhilinskii, *J. Mol. Spectrosc.* **103,** 147–159 (1984).
27. M. Badaoui and J. P. Champion, *J. Mol. Spectrosc.* **109,** 402–411 (1985).